XL CILAMCE
IBERO-LATIN AMERICAN CONGRESS ON COMPUTATIONAL METHODS IN ENGINEERING
NOVEMBER 11-14, 2019
Praiamar Natal Hotel & Convention Natal, RN-BRAZIL

BOUNDARY CONDITIONS FOR HIGH-ORDER LATTICE BOLTZMANN MODELS

Luiz Adolfo Hegele Júnior
Department of Petroleum Engineering, State University of Santa Catarina, Brazil
luiz.hegele@gmail.com
Keijo Kalervo Mattila
Department of Physics, University of Jyvaskyla, Jyvaskyla, Finland
k.kalervo.mattila@gmail.com
Jonas Hilbert Hegele
Mechanical Engineering Department, Federal University of Santa Catarina, Brazil
jonashegele@gmail.com
Ricardo Leite Martins Bazarin
Mechanical Engineering Department,Technological Federal University of Parana, Brazil
Ricardo_leitemartins@hotmail.com
Paulo Cesar Philippi
Mechanical Engineering Graduate Program, Pontifical Catholic University of Parana, Curitiba, Brazil paulo.philippi@pucpr.br

Abstract. In this work, lattice Boltzmann (LB) regularization is extended to boundary conditions (BC). Dealing with boundary conditions was ever considered a puzzling question in the LB method, especially, when a large set of lattice vectors is required for the description of a given physical problem in high order models. The most popular BC models are based on Ad-Hoc rules and, although these BC models were shown to be suitable for low-order LBE, their extension to high-order LBE was shown to be a very difficult problem and, at authors knowledge, never solved with satisfaction. In fact, the main question to be solved is how to deal with a problem when the number of unknowns (the particle populations coming from the outside part of the numerical domain) is greater than the number of equations we have at each boundary site. A new boundary condition model is here proposed. The main idea is that when we write both the equilibrium and non-equilibrium parts of the discrete populations in terms of its equilibrium and non-equilibrium hydrodynamic moments, these moments replace the discrete populations as unknowns, independently of the number of discrete velocities that are needed for solving a given problem. This idea is here applied to the 2D lid-driven cavity flow problem and improved stability properties are demonstrated.

1. Introduction

The lattice-Boltzmann equation (LBE) can be considered as a projection of the Boltzmann equation onto a subspace H_q of the Hilbert space H that maps the velocity space onto the real numbers. The dimension q of H_q is dependent on the hydrodynamic problem it is wanted to solve, whether isothermal or non-isothermal, or if it involves non-ideality in single or multi-component systems [1] [2], [3]. Since subspace H_q is generated by a finite Hermitian basis, truncated at a given order, the solution of a LBE involve errors being affected by high-order moments that cannot be controlled with this approximation and considered to contribute to instability issues. Regularization is not a new concept in LBM and dates to the pioneer works of Ladd [4] in 1994 showing to have improved stability properties by Latt & Chopard [5]. An improvement of the regularization method was proposed, in connection with kinetic projections, Mattila *et al*. [6], and it was demonstrated that solutions of the LB equations, with improved stability ranges, may be found in a systematic way, based on increasingly order projections of the continuous Boltzmann equation onto subspaces generated by a finite set of Hermite polynomials. We considered a particular truncation, filtering the diffusive parts of high-order non-equilibrium moments that do not belong to the Hilbert subspace H_q, retaining. only their corresponding advective parts that fit into this representation. The decomposition of moments into diffusive and advective parts is based directly on general relations between Hermite polynomial tensors. The resulting regularization procedure led to recurrence relations where high-order non-equilibrium moments were expressed in terms of low-order ones, Mattila *et al*. [6]. The procedure is appealing in the sense that stability can be enhanced without local variation of transport parameters, e.g., the viscosity, or without tuning the simulation parameters based on embedded optimization steps.

In this work, LB regularization is extended to boundary conditions (BC). While the regularization scheme leads to improved general stability of LBM [5], [6], it does not directly address boundary conditions. Most popular onsite boundary conditions solve for the unknown distributions using methods such as (i) bounce-back of the nonequilibrium distribution [7]; (ii) iterative scheme to solve for an unknown slip velocity [8]; (iii) extrapolation scheme based on non-equilibrium distribution functions [9]. However, the restriction to replacing a subset of the distributions leads to instability at even moderate Reynolds numbers [10]. Regularized onsite boundary conditions, which replace the entire distribution at the boundary, have been developed, but encounter instability at large Re and require complex iterative schemes to address edges and corners [10].

A new boundary condition model is here proposed. The main idea is that when we write both the equilibrium and non-equilibrium parts of the discrete populations f_i in terms of its equilibrium and non-equilibrium hydrodynamic moments, these moments replace the discrete populations as unknowns, independently of the number of discrete velocities that are needed for solving a given problem. This idea is applied to the 2D lid-driven cavity flow problem and improved stability properties are demonstrated.

2. The LB equation as a kinetic projection

The distribution $f(\mathbf{x},\boldsymbol{\xi},t)$, solution of the Boltzmann equation

$$\partial_t f + \boldsymbol{\xi}\cdot\nabla f = \Omega \ , \tag{1}$$

may be considered, for each $(\mathbf{x},t)$ as a map from the continuous velocity space ξ^D onto the space $\mathcal{R}$ of real numbers (Figure 1). In fact, it belongs to the Hilbert space $\mathcal{H}$ of square integrable functions $f:\xi^D\to\mathcal{R}$ and may be written in terms of an orthogonal basis of $\mathcal{H}$ that will be, here, considered as the infinite set of Hermite polynomial tensors,

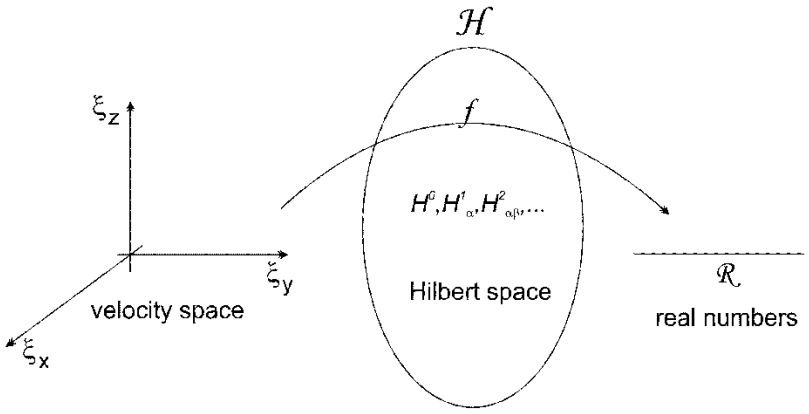

Figure 1. The Hilbert space solution of the Boltzmann equation.

Consider now the subspace $\mathcal{H}_q$ of $\mathcal{H}$ generated by a finite set of q Hermite polynomial tensors (Figure 2). The projection of the Boltzmann equation, Eq. (1) onto this subspace will have a solution that can be written in its dimensionless form as,

$$\overline{f} = \frac{f\overline{\xi}^D}{n_0} = \frac{e^{-\frac{\xi_0^2}{2}}}{(2\pi)^{\frac{D}{2}}} \sum_{H^{(\theta)} \in \mathcal{H}_q} \frac{a^{(\theta)}}{n_x! n_y! n_z!} H^{(\theta)} \quad . \tag{2}$$

Notation is standard. The dimensionless molecular velocity is given by $\boldsymbol{\xi}_0 = \boldsymbol{\xi} / \overline{\xi}$, where $\overline{\xi} = \sqrt{kT_0 / m}$, is related to the average molecular speed, T_0 is a reference temperature, m is the mass of a single molecule, n_0 is a reference number density of molecules and k is the Boltzmann constant. Symbols n_x, n_y, n_z means the number of times the index $\alpha = n_x, n_y, n_z$ appears repeated in the Hermite polynomial tensor, $n_x + n_y + n_z = \theta$ and $e^{-\frac{\xi_0^2}{2}} \Big/ (2\pi)^{\frac{D}{2}}$ is the weight function for the Hermite polynomials.

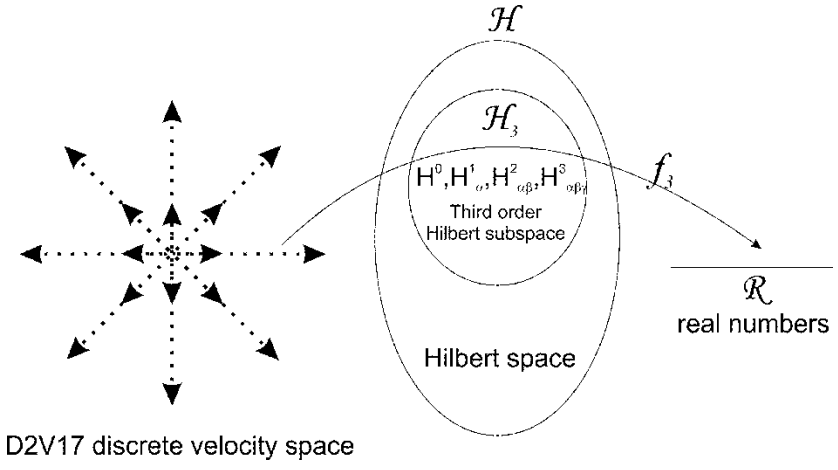

Figure 2. Subspace $\mathcal{H}_{q=10}$ of $\mathcal{H}$ generated by a finite set of 10 Hermite polynomial tensors and related to the D2V17 LBE [12].

The subspace $\mathcal{H}_q$ is directly related to the set of b discrete velocities $\xi_{0,i}$, $i = 0,....,b-1$ used to represent the velocity space This formal relationship was found by Philippi and co-workers [12], [13] and Shan et al. [14] and is based on the preservation of the inner product

$$\left(H^{(\theta)} * H^{(\eta)}\right)_d = \left(H^{(\theta)} * H^{(\eta)}\right)_c \ , \tag{3}$$

between any two Hermite polynomials $H^{(\theta)}$, $H^{(\eta)}$ that form the basis of $\mathcal{H}_q$, where

$$\left(H^{(\theta)} * H^{(\eta)}\right)_c = \frac{1}{(2\pi)^{\frac{D}{2}}} \int e^{-\frac{\xi_0^2}{2}} H^{(\theta)}(\xi_0) * H^{(\eta)}(\xi_0) d\xi_0 \ , \tag{4}$$

and

$$\left(H^{(\theta)} * H^{(\eta)}\right)_d = \sum_i W_i H^{(\theta)}(a_s \mathbf{e}_i) * H^{(\eta)}(a_s \mathbf{e}_i) \ . \tag{5}$$

In the above equations, W_i are quadrature weights and a_s is the scaling factor that relates the lattice vectors $\mathbf{e}_i$ to the dimensionless velocities, $\xi_{0,i} = a_s \mathbf{e}_i$. Since the Hermite polynomials are orthogonal in the continuous velocity space, the above condition means that, when considered as mappings from the discrete velocity space onto the real numbers, their inner product must be zero or the square of their norm, when identical,

$$\sum_i W_i \left(H^{(\theta)}(a_s \mathbf{e}_i)\right)^2 = \frac{1}{(2\pi)^{\frac{D}{2}}} \int e^{-\frac{\xi_0^2}{2}} \left(H^{(\theta)}(\xi_0)\right)^2 d\xi_0 \ . \tag{6}$$

The above relationship results in a set of equations for each $H^{(\theta)} \in \mathcal{H}_q$, that can be solved for the scaling factor a_s and weights W_i.

The collision term Ω in Eq. (1), is usually written as a BGK relaxation term [15]. In dimensionless form

$$\bar{\Omega} = -\frac{\bar{f} - \bar{f}^{eq}}{\tau^*} \ , \tag{7}$$

where the Maxwell-Boltzmann equilibrium distribution can be written, in its dimensionless form, as

$$\bar{f}^{eq} = \rho^* \frac{1}{(2\pi)^{\frac{D}{2}}} \frac{e^{-\frac{(\xi_0 - u_o)^2}{2(\Theta+1)}}}{(\Theta+1)^{\frac{D}{2}}} \ , \tag{8}$$

where $\rho^* = n / n_0$ and $\Theta = T/T_0 - 1$ is the local temperature deviation from the reference temperature T_0.

In subspace $\mathcal{H}_q$ the MB equilibrium distribution is to be written in terms of the finite set of Hermite polynomial tensors spanning $\mathcal{H}_q$

$$\bar{f}^{eq} = \frac{e^{-\frac{\xi_0^2}{2}}}{(2\pi)^{\frac{D}{2}}} \sum_{H^{(\theta)} \in \mathcal{H}_q} \frac{a_{eq}^{(\theta)}}{n_x! n_y! n_z!} H^{(\theta)} \ . \tag{9}$$

In its discrete form, Eq. (1) can be written as

$$\partial_t \overline{f}_i + \boldsymbol{\xi}_i \cdot \nabla \overline{f}_i = -\frac{\overline{f}_i - \overline{f}_i^{eq}}{\tau} \ , \tag{10}$$

where $\overline{f}_i = \overline{f}\left(\mathbf{x}, \boldsymbol{\xi}_i, t\right)$, $i = 0,....,b-1$, are the populations of particles that, at time *t*, have a velocity $\boldsymbol{\xi}_i$ in site $\mathbf{x}$, $t^* = t/\delta$, δ is the time step, $\nabla^* = \nabla/h$ and h is the orthogonal distance between two contiguous sites.

Using a first order Taylor expansion for $\overline{f}_i$,

$$\overline{f}_i\left(\mathbf{x} + \Delta\mathbf{x}, t + \delta\right) - \overline{f}_i\left(\mathbf{x}, t\right) = \delta\partial_t \overline{f}_i + \Delta\mathbf{x} \cdot \nabla\overline{f} + O\left(\delta^2, \left|\Delta\mathbf{x}\right|^2\right) . \tag{11}$$

When $\Delta\mathbf{x} = \boldsymbol{\xi}_i\delta$, meaning that the velocities $\boldsymbol{\xi}_i$ are chosen in such a way that particles are propagated to next neighbor sites (a CFL number equal to 1), the above equation reduces to

$$\overline{f}_i\left(\mathbf{x} + \boldsymbol{\xi}_i\delta, t + \delta\right) - \overline{f}_i\left(\mathbf{x}, t\right) = \delta\left(\partial_t \overline{f}_i + \boldsymbol{\xi}_i \cdot \nabla\overline{f}\right) + O\left(\delta^2\right) \tag{12}$$

and by defining $\omega = \delta/\tau$, Eq. (10) can be rewritten as

$$\overline{f}_i\left(\mathbf{x} + \mathbf{e}_i h, t + \delta\right) - \overline{f}_i\left(\mathbf{x}, t\right) = -\omega\left(\overline{f}_i - \overline{f}_i^{eq}\right) + O\left(\delta^2\right) \tag{13}$$

or, in the form,

$$\overline{f}_i\left(\mathbf{x} + \mathbf{e}_i h, t + \delta\right) = \overline{f}_i^{eq}\left(\mathbf{x}, t\right) + \left(1 - \omega\right)\overline{f}_i^{neq} + O\left(\delta^2\right) \tag{14}$$

2.1. Moments

From Eq. (9), the first Hermitian equilibrium moments are

$$\begin{aligned} a_{eq}^{(0)} &= \int \overline{f}^{eq} \times H^{(0)} d\boldsymbol{\xi}_0 = \rho^* \\ a_{eq,\alpha}^{(1)} &= \int \overline{f}^{eq} \times H_\alpha^{(1)} d\boldsymbol{\xi}_0 = \rho^* a_s u_\alpha^* \\ a_{eq,\alpha\beta}^{(2)} &= \int \overline{f}^{eq} \times H_{\alpha\beta}^{(2)} d\boldsymbol{\xi}_0 = \rho^*\left(a_s^2 u_\alpha^* u_\beta^* + \Theta\delta_{\alpha\beta}\right) \end{aligned} \ , \tag{15}$$

where $u_\alpha^* = a_s u_{0,\alpha}$.

In the same way, the Hermitian non-equilibrium moments can be found from Eq. (2)

$$\begin{aligned} a_{neq}^{(0)} &= \int \overline{f}^{neq} \times H^{(0)} d\boldsymbol{\xi}_0 = 0 \\ a_{neq,\alpha}^{(1)} &= \int \overline{f}^{neq} \times H_\alpha^{(1)} d\boldsymbol{\xi}_0 = 0 \end{aligned} \ . \tag{16}$$

The second order non-equilibrium moment

$$\begin{aligned} a_{neq,\alpha\beta}^{(2)} &= \int \overline{f}^{neq} \times H_{\alpha\beta}^{(2)} d\boldsymbol{\xi}_0 = \int \overline{f}^{neq} \times \left(\xi_{0,\alpha}\xi_{0,\beta} - \delta_{\alpha\beta}\right) d\boldsymbol{\xi}_0 \\ &= \int \overline{f}^{neq} \times \xi_{0,\alpha}\xi_{0,\beta} d\boldsymbol{\xi}_0 \end{aligned} \tag{17}$$

is directly related to the dimensionless viscous stress tensor

$$\begin{aligned}\tau_{\alpha\beta} &= \int f^{neq} m\left(\xi_\alpha - u_\alpha\right)\left(\xi_\beta - u_\beta\right) d\xi \\ &= \rho_0 \overline{\xi}^2 \int \frac{\overline{\xi}^D f^{neq}}{n_0} \xi_{0,\alpha}\xi_{0,\beta} d\xi_0 \\ &= \rho_0 \overline{\xi}^2 \int \overline{f}^{neq} \xi_{0,\alpha}\xi_{0,\beta} d\xi_0\end{aligned} \quad . \tag{18}$$

The dimensionless velocity $\overline{\xi} = \frac{c^2}{a_s^2}$ with $c = h/\delta$ representing the lattice speed, in such a way that

$$\tau^*_{\alpha\beta} = \frac{\tau_{\alpha\beta}}{\rho_0 c^2} = \frac{1}{a_s^2}\int \overline{f}^{neq} \xi_{0,\alpha}\xi_{0,\beta} d\xi_0 = \frac{1}{a_s^2} a^{(2)}_{neq,\alpha\beta} \tag{19}$$

or, as it is more usual to write

$$a^{(2)}_{neq,\alpha\beta} = \frac{\tau^*_{\alpha\beta}}{c_s^2} \tag{20}$$

where $c_s = 1/a_s$ is the dimensionless speed of sound in isothermal systems.

3. The D2Q9 LBE

Let us consider a two dimensional second-order Hermitian representation as shown in Figure 3.

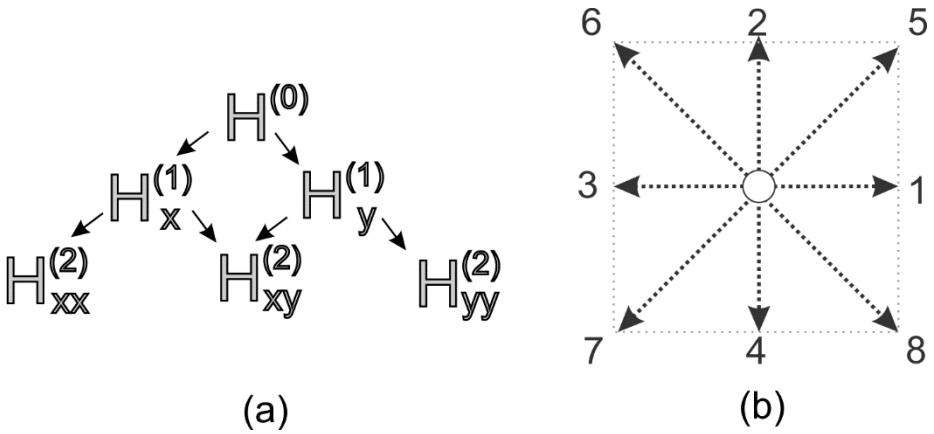

Figure 3. (a) Second-order Hermitian basis of the D2Q9 LBE (b).

The norm preservation condition, Eq. (6) gives a set of 4 independent equations for the weights and scaling factor, whose solution is

$$W_0 = 16/36, W_1 = W\left(|e_i| = 1\right) = 4/36, W_2 = \left(|e_i| = \sqrt{2}\right) = 1/36, a_s = \sqrt{3}.$$

The equilibrium distribution is given by Eq. (9). In isothermal condition $\left(\Theta = 0\right)$,

$$\begin{aligned}\overline{f}_{i,q=6}^{eq} &= W_i\left[\begin{array}{l} a_{eq}^{(0)}H^{(0)} + a_{eq,x}^{(1)}H_x^{(1)} + a_{eq,y}^{(1)}H_y^{(1)} \\ +\frac{1}{2}a_{eq,xx}^{(2)}H_{xx}^{(2)} + a_{eq,xy}^{(2)}H_{xy}^{(2)} + \frac{1}{2}a_{eq,yy}^{(2)}H_{yy}^{(2)} \end{array}\right] \\ &= \rho^* W_i\left[1 + a_s^2 u_\alpha^* e_{i\alpha} + \frac{1}{2}a_s^2 u_\alpha^* u_\beta^*\left(a_s^2 e_{i\alpha}e_{i\beta} - \delta_{\alpha\beta}\right)\right]\end{aligned}, \tag{21}$$

In the same way the non-equilibrium distribution may be written as

$$\begin{aligned}\overline{f}_i^{neq} &= W_i\left[\begin{array}{l} a_{neq}^{(0)}H^{(0)} + a_{neq,x}^{(1)}H_x^{(1)} + a_{neq,y}^{(1)}H_y^{(1)} \\ +\frac{1}{2}a_{neq,xx}^{(2)}H_{xx}^{(2)} + a_{neq,xy}^{(2)}H_{xy}^{(2)} + \frac{1}{2}a_{neq,yy}^{(2)}H_{yy}^{(2)} \end{array}\right], \\ &= W_i\left[\frac{1}{2}a_s^2\tau_{\alpha\beta}^*\left(a_s^2 e_{i\alpha}e_{i\beta} - \delta_{\alpha\beta}\right)\right]\end{aligned} \tag{22}$$

because, from Eq. (16), the zero-th and first order Hemitian moments are null.

Second-order LBE such as the D2Q9 and its counterparts D1Q3 in one-dimensional systems and D3Q27 in three-dimensions do not preserve energy. Consequently, the condition

$$\frac{1}{2}\sum_i \overline{f}_i^{neq} e_i^2 = \frac{1}{2}\left(\tau_{xx}^* + \tau_{yy}^*\right) = 0 \ , \tag{23}$$

cannot be verified. From fluid mechanics theory, Eq. (23) is recognized as the Stokes assumption of zero bulk viscosity, a condition that must be satisfied by kinetic models in the framework of the Boltzmann equation, based on material points, because the first and second viscosity coefficients are identical for such systems. Indeed, a careful Chapman-Enskog analysis of the D2Q9 LBE leads to

$$\tau_{xx}^* + \tau_{yy}^* = -\frac{2}{3\omega}\rho^*\nabla\cdot\mathbf{u} \ .$$

and the Stokes condition can be only satisfied for incompressible flows, when $\nabla\cdot\mathbf{u} = 0$.

In addition, second-order non-equilibrium moments such as $\tau_{\alpha\beta}^*$ are dependent on the spatial derivatives of *third-order equilibrium moments* [6]. Therefore, the full set of third-order Hermite polynomials, $H_{xxx}^{(3)}, H_{xxy}^{(3)}, H_{xyy}^{(3)}, H_{yyy}^{(3)}$, is required in the Hermitian basis of a LBE as a necessary condition for retrieving the hydrodynamic Navier-Stokes (NS) equations in isothermal conditions ($\Theta = 0$). These Hermite polynomials are not present in the Hermitian representation given in Figure 3 and, in consequence, the NS equations will be only retrieved with third-order errors $O\left(u^3\right)$. Since the Mach number $Ma = u^*/c_s$, the usual strategy is to keep the Mach number as small as possible limiting the simulations to the quasi-incompressible limit. The inconvenient of this strategy is the increase in the computational costs, because the Reynolds number

$$\mathrm{Re} = \frac{u^* N}{c_s^2\left(\frac{1}{\omega} - \frac{1}{2}\right)} \ , \tag{24}$$

can be only increased by increasing the resolution *N* of the simulation domain, when the relaxation frequency ω cannot be further increased approaching its upper limit, $\omega = 2$, for preventing instability issues.

4. Collision and propagation steps

After propagation the populations $\overline{f}_i$ are known in every fluid site of the numerical domain. The dimensionless density and local velocity are calculated in accordance with

$$\begin{aligned} \rho^* &= \sum_i \overline{f}_i \\ \rho^* u_\alpha^* &= \sum_i \overline{f}_i e_{i\alpha} \end{aligned} \quad , \tag{25}$$

and the equilibrium populations $\overline{f}_i^{eq}\left(\rho^*, u_x^*, u_y^*\right)$ in accordance with Eqs. (21).

For each direction *i*, the non-equilibrium populations are given by

$$\overline{f}_i^{neq} = \overline{f}_i - \overline{f}_i^{eq} \ . \tag{26}$$

The main idea of the regularization method for collision-propagation schemes is that the non-equilibrium populations calculated with Eq. (26) cannot be supposed to be free of errors due to higher-order *ghost* moments that cannot be controlled, considering the order of approximation of the kinetic projection to the Boltzmann equation.

It is now time to calculate the components of the viscous stress tensor

$$\tau_{\alpha\beta}^* = \sum_i \overline{f}_i^{neq} e_{i\alpha} e_{i\beta} \ , \tag{27}$$

and to filter the noise produced by numerical errors due to non-controlled higher-order moments. This is performed by recalculating the non-equilibrium populations in accordance with Eq. (22)

$$\hat{\overline{f}}_i^{neq} = W_i \left[\frac{1}{2} a_s^2 \tau_{\alpha\beta}^* \left(a_s^2 e_{i\alpha} e_{i\beta} - \delta_{\alpha\beta} \right) \right] . \tag{28}$$

This procedure is to be seen as a *regularization* step since, at each time step, it is not in our interest to take the information for $\overline{f}_i^{neq}$ given by Eq. (26) into account, because it cannot be supposed to be free of errors that will affect the accuracy and stability of the algorithm.

The numerical values of the equilibrium $\overline{f}_i^{eq}$ and *regularized* non-equilibrium populations $\hat{\overline{f}}_i^{neq}$ are required in each site $\mathbf{x}$ for performing the collision step, when all populations are recalculated in accordance with

$$\overline{f}_i^{out}\left(\mathbf{x}, t\right) = \overline{f}_i^{eq} + \left(1-\omega\right) \hat{\overline{f}}_i^{neq} \ . \tag{29}$$

Populations $\overline{f}_i^{out}$ are then propagated to neighbor sites in accordance with

$$\overline{f}_i \ \left(\mathbf{x} + \mathbf{e}_i h, t + \delta\right) = \overline{f}_i^{out}\left(\mathbf{x}, t\right) \tag{30}$$

5. Boundary conditions for second order LBE

Consider the wet node located in $\left(x_b, y_b\right)$ adjacent to the solid surface in Figure 4 and suppose that the populations that are shown in black in the figure are the populations that were propagated to $\left(x_b, y_b\right)$ from neighbor fluid sites. Populations $f_4, f_7, f_8,$ shown in red are unknown.

Since the node (x_b, y_b) is a fluid site, we can write the post-collisional populations in accordance with Eq. (14)

$$\hat{\bar{f}}_i^{out}(\mathbf{x},t) = \bar{f}_i^{eq}\left(\rho^*, u_x^*, u_y^*\right) + (1-\omega)\,\hat{\bar{f}}_i^{neq}\left(\tau_{xx}^*, \tau_{xy}^*, \tau_{yy}^*\right) . \tag{31}$$

Independently of the number of lattice vectors in the representation, when the velocity of the boundary node is known, the only unknowns are the density ρ^* and the 3 components of the viscous stress tensor $\tau_{xx}^*, \tau_{xy}^*, \tau_{yy}^*$ in this kind of problem.

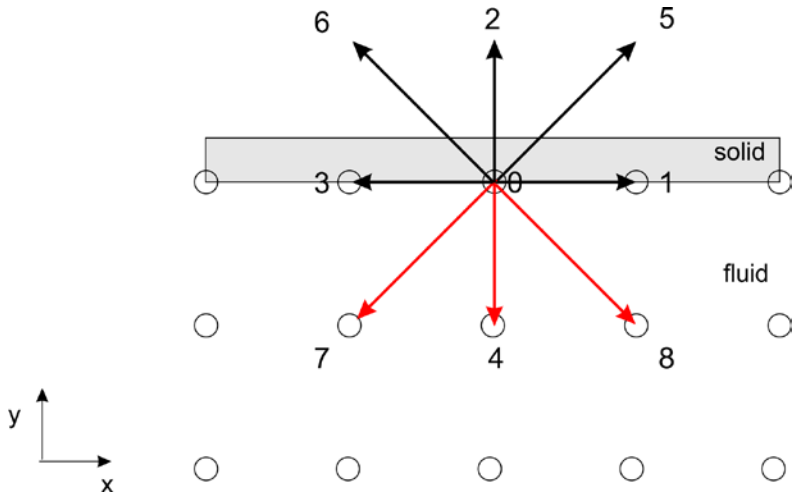

Figure 4. A wet node adjacent to a solid surface.

5.1 Mass conservation

Since mass must be conserved and node (x_b, y_b) is adjacent to a solid surface, the sum of the populations of particles outgoing from the boundary node to the fluid sites after the collision step, must be identical to the sum of the populations incoming from fluid sites before the collision step, or

$$\sum_{i\in I} \bar{f}_i = \sum_{i\in O} \bar{f}_i^{out} \tag{32}$$

where $I = \{0,1,2,3,5,6\}$ and $O = \{0,1,3,4,7,8\}$ are, respectively, the sets of outgoing and incoming directions from and to the fluid sites.

Populations $\bar{f}_i^{out}$ are now replaced by their kinetic projections $\hat{\bar{f}}_i^{out}$ for $i \notin I$, corresponding to populations f_4, f_7, f_8 in Figure 4. Recall that the l.h.s. of Eq. (32) is a known positive real number and that, after this replacement, the r.h.s of this equation has a linear dependence on ρ^*, $\tau_{xx}^*, \tau_{xy}^*, \tau_{yy}^*$.

For the node depicted in Figure 4, this condition results in the following equation,

$$\left(\frac{1}{6} + \frac{2}{3}\omega - \frac{1}{2}u_y^* - \left(\omega - \frac{1}{2}\right)u_y^{*2}\right)\rho^* - \frac{1}{2}(\omega-1)\tau_{yy}^* = A\ , \tag{33}$$

where $\omega = 1/\tau^*$ is a collision frequency and $A = \omega\left(\overline{f}_0 + \overline{f}_1 + \overline{f}_3\right) + \overline{f}_2 + \overline{f}_5 + \overline{f}_6$ is a real number that depends on $(\mathbf{x}_b, t)$.

5.2 Solution based on the regularization of second-order moments

For a Dirichlet boundary condition such as the one we have when the boundary node velocity is prescribed, a suitable approach to the boundary condition problem is to write the second-order non-equilibrium moments τ^*_{xx}, τ^*_{yy} and τ^*_{xy} in terms of regularized populations, in such a way as to assure the mass conservation and non-slip conditions.

Mass conservation is assured by Eq. (32). Adherence condition can be assured by prescribing the velocity of the boundary node. The idea is, here, to produce a solution based on the regularization of components τ^*_{xx}, τ^*_{yy} and τ^*_{xy} of the viscous stress tensor. This appears to be a natural choice for a Dirichlet BC, since adherence is still required for all boundary sites.

So we write τ^*_{xx}, τ^*_{yy} and τ^*_{xy} in accordance with

$$\begin{aligned}\tau^*_{\alpha\beta} &= \sum_{i\in I}\overline{f}_i^{neq} e_{i\alpha}e_{i\beta} + \sum_{i\notin I}\hat{\overline{f}}_i^{neq} e_{i\alpha}e_{i\beta} \\ &= \sum_{i\in I}\overline{f}_i\, e_{i\alpha}e_{i\beta} - \sum_{i\in I}\overline{f}_i^{eq}\left(\rho^*\right)e_{i\alpha}e_{i\beta} + \sum_{i\notin I}\hat{\overline{f}}_i^{neq}\left(\tau^*_{xx},\tau^*_{xy},\tau^*_{yy}\right)e_{i\alpha}e_{i\beta},\end{aligned} \tag{34}$$

and get the following equations

$$\begin{aligned}&\rho^* u^*_x\left(\frac{1}{6}+\frac{1}{2}u^*_y\left(u^*_y+1\right)\right)+\frac{1}{2}\tau^*_{yy} = B,\\ &\frac{\rho^*}{6}\left(\frac{5}{3}+\left[u^*_y\left(u^*_y+1\right)+u^{*2}_x\right]\right)+\frac{5}{6}\tau^*_{xx}-\frac{1}{6}\tau^*_{yy} = C,\\ &\rho^* u^*_x\left(\frac{1}{6}+\frac{1}{2}u^*_y\right)+\frac{1}{2}\tau^*_{xy} = D,\end{aligned} \tag{35}$$

where $B = \overline{f}_2 + \overline{f}_5 + \overline{f}_6$, $C = \overline{f}_1 + \overline{f}_3 + \overline{f}_5 + \overline{f}_6$ and $D = \overline{f}_5 - \overline{f}_6$.

The solution of Eqs. (33) and (35) results into the following relations

$$\begin{aligned}&\rho^* = 6\omega\frac{\overline{f}_0+\overline{f}_1+\overline{f}_2+\overline{f}_3+\overline{f}_5+\overline{f}_6}{5\omega-3\left[(2-\omega)u^*_y+\omega u^{*2}_y\right]},\\ &\tau^*_{yy} = 2\left(\overline{f}_2+\overline{f}_5+\overline{f}_6\right)-\rho^*\left[u^*_y\left(u^*_y+1\right)+\frac{1}{3}\right],\\ &\tau^*_{xx} = \frac{2}{5}\left(3\overline{f}_1+\overline{f}_2+3\overline{f}_3+4\overline{f}_5+4\overline{f}_6\right)-\frac{1}{5}\rho^*\left[2+2u^*_y\left(u_y+1\right)+5u^{*2}_x\right],\\ &\tau^*_{xy} = 2\left(\overline{f}_5-\overline{f}_6\right)-\rho^* u^*_x\left(u^*_y+\frac{1}{3}\right).\end{aligned} \tag{36}$$

The unknown populations $\overline{f}_i,\ i\notin I$ can be now written in terms of the incoming populations $\overline{f}_i,\ i\in I$ by using

$$\overline{f}_i = \overline{f}_i^{eq} + \hat{\overline{f}}_i^{neq}\ , \tag{37}$$

for $i \notin I$, in this case, populations $\overline{f}_4, \overline{f}_7, \overline{f}_8$. The following equations are obtained

$$\begin{aligned}
\overline{f}_4 &= \frac{1}{15}\left(\rho^* - 3\overline{f}_1 + 9\overline{f}_2 - 3\overline{f}_3 + 6\overline{f}_5 + 6\overline{f}_6 - 9\rho^* u_y^* + \rho^* u_y^{*2}\right), \\
\overline{f}_7 &= -\frac{1}{30}\left(\rho^* - 3\overline{f}_1 - 6\overline{f}_2 - 3\overline{f}_3 - 24\overline{f}_5 + 6\overline{f}_6 + 5\rho^* u_x^* + 6\rho^* u_y^* + \rho^* u_y^{*2}\right), \\
\overline{f}_8 &= -\frac{1}{30}\left(\rho^* - 3\overline{f}_1 - 6\overline{f}_2 - 3\overline{f}_3 + 6\overline{f}_5 - 24\overline{f}_6 - 5\rho^* u_x^* + 6\rho^* u_y^* + \rho^* u_y^{*2}\right).
\end{aligned} \tag{38}$$

Consistency

Consider the sample case where the boundary node is at rest $\left(u_x^*(\mathbf{x}_b,t) = u_y^*(\mathbf{x}_b,t) = 0\right)$. In collision-propagation framework every boundary condition problem involves the determination of a set of unknown pre-collisional populations $\overline{f}_i$. After the collision step, these populations propagate the information on the physical state of the boundary to next neighbor sites, inside the fluid phase. Under the continuum hypothesis, the Knudsen number is close to zero, $Kn \to 0$, meaning that collisions are dominant. In these local collision processes, outgoing particles from the boundary transfer the information that says that the local velocity is zero at the boundary to the particles that are incoming from fluid phase.

When we add the populations $\overline{f}_4, \overline{f}_7, \overline{f}_8$ given by Eq. (38), we get

$$\overline{f}_4 + \overline{f}_7 + \overline{f}_8 = \rho^* u_y^* - \overline{f}_2 - \overline{f}_5 - \overline{f}_6 \quad . \tag{39}$$

This equation can be rewritten as

$$\overline{f}_2 + \overline{f}_5 + \overline{f}_6 - \overline{f}_4 - \overline{f}_7 - \overline{f}_8 = \rho^* u_y^* \ , \tag{40}$$

which is consistent with the statistical definition of the normal component of the momentum

$$\sum_i \overline{f}_i e_{iy} = \rho^* u_y^* \ .$$

By adding the populations $\overline{f}_i(\mathbf{x}_b,t)$, replacing $\overline{f}_4, \overline{f}_7, \overline{f}_8$ by their expressions in terms of the known incoming populations given by Eq. (38), the following equation is obtained

$$\sum_i \overline{f}_i = \overline{f}_0 + \overline{f}_1 + 2\overline{f}_2 + \overline{f}_3 + 2\overline{f}_5 + 2\overline{f}_6 - \rho^* u_y^* \ , \tag{41}$$

which can be rewritten as

$$\begin{aligned}
\sum_i \overline{f}_i = \overline{f}_0 + \overline{f}_1 + \overline{f}_2 + \overline{f}_3 + \overline{f}_5 + \overline{f}_6 + \overline{f}_4 + \overline{f}_7 + \overline{f}_8 \\
+ \overline{f}_2 + \overline{f}_5 + \overline{f}_6 - \overline{f}_4 - \overline{f}_7 - \overline{f}_8 - \rho^* u_y^*
\end{aligned} \ , \tag{42}$$

and, since from Eq. (40) we know that the second part on the r.h.s. of Eq. (42) is null, this result is consistent with the statistical definition of density at the boundary node $\mathbf{x}_b$.

$$\sum_i \overline{f}_i = \rho^* \ . \tag{43}$$

Consider now that population $\overline{f}_7$ is subtracted from population $\overline{f}_8$ in Eq. (38). The following result is obtained

$$\overline{f}_8 - \overline{f}_7 = \overline{f}_6 - \overline{f}_5 + \frac{1}{3}\rho^* u_x^* \,, \tag{44}$$

which can be rewritten as

$$\overline{f}_8 - \overline{f}_7 - \overline{f}_6 + \overline{f}_5 = \frac{1}{3}\rho^* u_x^* . \tag{45}$$

To be consistent with the statistical definition of the x-component of the momentum, the difference $\overline{f}_1 - \overline{f}_3$ should be equal to $\frac{2}{3}\rho^* u_x^*$, which is exactly the result we get when regularized forms of $\overline{f}_1$ and $\overline{f}_3$ are used.

Therefore, Eq. (37)

$$\overline{f}_i = \overline{f}_i^{eq} + \hat{\overline{f}}_i^{neq}$$

is used for *all populations* $\overline{f}_i,\ i = 0,...,8$ expressing both the unknown and known populations in terms of the density ρ^* and the second order moments $\tau_{xx}^*, \tau_{xy}^*, \tau_{yy}^*$, given by Eq. (36). This means that the incoming populations are also replaced by their regularized forms on the boundary sites. So, errors produced by high order moments are also avoided on the boundary nodes, with appreciable results on the stability of the algorithm.

Eq. (43) and the adherence conditions

$$\sum_i \overline{f}_i e_{ix} = \rho^* u_x^*, \quad \sum_i \overline{f}_i e_{iy} = \rho^* u_y^*$$

lead to a system of 3 equations for 4 unknowns $\overline{f}_4, \overline{f}_7, \overline{f}_8$ and ρ^*. This is the main difficulty of some former methods for solving the BC equations and, in previous work, this system was solved by using *ad-hoc* assumptions. This is the case of Zou and He [7] and Inamuro [8] models and the assumption of bounce-back reflection. In contrast, the use of regularized forms for the populations $\overline{f}_i,\ i \notin I$ leads to the solution of the boundary condition problem without any heuristic assumptions. This is especially important when we deal with high-order sets of lattice-vectors [12].

5.3. Corner sites

The procedure based on the replacement of the unknown populations by their kinetic projections written in terms of ρ^* and second order non equilibrium moments may be extended to corner and edge sites in 2D and 3D problems.

Consider, for instance, the 2D corner site of Figure 5. Populations $\overline{f}_1, \overline{f}_4, \overline{f}_8, \overline{f}_5, \overline{f}_7$ are unknown and should be replaced by their kinetic projections. In this case, the set related to the incoming populations is $I = \{0,2,3,6\}$ and set $O = \{0,1,4,8\}$ designate the outgoing directions from the boundary node to the fluid phase. Therefore, populations $\overline{f}_5, \overline{f}_7$ do not have any role in the calculation of the unknown values of the pre-collisional populations $\overline{f}_1, \overline{f}_4, \overline{f}_8$ from the known values of populations $\overline{f}_0, \overline{f}_2, \overline{f}_3, \overline{f}_6$.

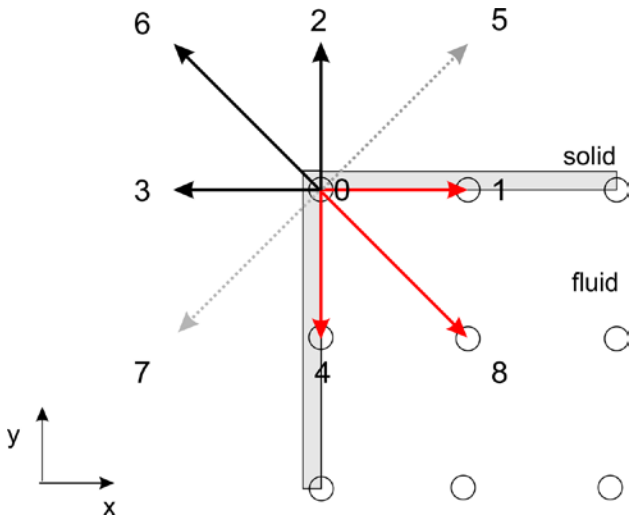

Figure 5. A corner site. Populations $\overline{f}_1, \overline{f}_4, \overline{f}_8, \overline{f}_5, \overline{f}_7$ are unknown and replaced by their kinetic projections.

For finding the unknown populations, the procedure is exactly the same as in Section 5.2. We require the conservation of mass, Eq. (32) and the regularization condition, Eq. (34) for the second order moments $\tau_{xx}, \tau_{yy}, \tau_{xy}$. When the corner site is at rest, we find

$$\begin{aligned}
\rho^* &= \frac{36}{451\omega+24}\left[\left(19\overline{f}_0+15\overline{f}_2+15\overline{f}_3+27\overline{f}_6\right)\omega+4\overline{f}_2+4\overline{f}_3-8\overline{f}_6\right] \\
\tau_{xx}^* &= \frac{2}{451\omega+24}\left[\left(-156\overline{f}_0+43\overline{f}_2+494\overline{f}_3+348\overline{f}_6\right)\omega-24\overline{f}_2+96\overline{f}_6\right] \\
\tau_{xy}^* &= \frac{6\omega}{451\omega+24}\left(6\overline{f}_0-19\overline{f}_2-19\overline{f}_3+56\overline{f}_6\right) \\
\tau_{yy}^* &= \frac{2\omega}{451\omega+24}\left[\left(-156\overline{f}_0+494\overline{f}_2+43\overline{f}_3+348\overline{f}_6\right)\omega-24\overline{f}_3+96\overline{f}_6\right]
\end{aligned} . \qquad (46)$$

Using Eq. (37), identical expressions are found for populations $\overline{f}_5, \overline{f}_7$,

$$\overline{f}_5 = \overline{f}_7 = \frac{1}{233\omega+42}\left[4\omega\overline{f}_0+(6+23\omega)\overline{f}_2+(6+23\omega)\overline{f}_3-(6+15\omega)\overline{f}_6\right], \qquad (47)$$

5.5. Wet node at the entrance/exit of the fluid domain

Consider now that the solid surface is replaced by a fluid domain representing a fluid that is flowing into/out the numerical domain of interest from the outside/inside (Figure 6). In these cases, populations $\overline{f}_4, \overline{f}_7, \overline{f}_8$ came from outside and are unknown. In contrast with the previous case, there is no mass conservation on node $\mathbf{x}_b$, because we have fluid from outside being added/withdrawn to/from the fluid domain, assuring a fluid velocity $\mathbf{u}(\mathbf{x}_b, t)$ along the entrance/exit of the numerical domain. In many cases, it is desirable to simulate a uniform and constant velocity field of velocity $u_y = const.$, $u_x = 0$, as it happens when the boundary surface (or line in 2D problems) is the entrance of a wind tunnel.

In these cases, populations $\overline{f}_i$ must satisfy Eq.(43) . Remark that the velocity components u_x^* and u_y^* are considered to be known and density ρ^* has, here, the role of the pressure at the entrance/exit node

$$P^* = c_s^2 \rho^* ,$$

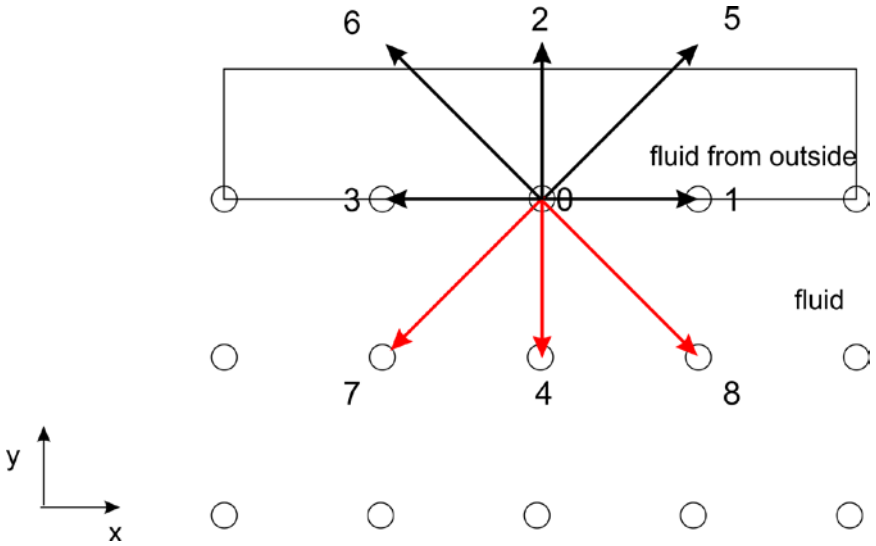

Figure 6. Wet node in the entrance/exit of the fluid domain.

and populations $\overline{f}_i$ are expected to satisfy

$$\sum_i \overline{f}_i = \rho^* \ , \tag{48}$$

which can be written as

$$\sum_{i\in I} \overline{f}_i + \sum_{i\notin I} \hat{\overline{f}}_i = \rho^* \ . \tag{49}$$

Replacing $\overline{f}_i,\ i \notin I$ by their kinetic projections, the following relationship is obtained

$$\rho^*\left(\frac{5}{6}+\frac{1}{2}u_y^*\left(1-u_y^*\right)\right)-\frac{1}{2}\tau_{yy}^* = A_1 \ , \tag{50}$$

where $A_1 = \overline{f}_0 + \overline{f}_1 + \overline{f}_2 + \overline{f}_3 + \overline{f}_5 + \overline{f}_6$.

Solution of Eqs. (34) and (50) gives

$$\begin{aligned}
\rho^* &= \frac{1}{u_y^*+1}\left(\overline{f}_0 + \overline{f}_1 + 2\overline{f}_2 + \overline{f}_3 + 2\overline{f}_5 + 2\overline{f}_6\right),\\
\tau_{xx}^* &= -\frac{1}{5}\left(2\overline{f}_0 - 4\overline{f}_1 + 2\overline{f}_2 - 4\overline{f}_3 - 4\overline{f}_5 - 4\overline{f}_6 + 5\rho^* u_x^{*2} + 2\rho^* u_y^{*2}\right),\\
\tau_{yy}^* &= \rho^*\left[u_y^*\left(1-u_y^*\right)+\frac{5}{3}\right] - 2\left(\overline{f}_0 + \overline{f}_1 + \overline{f}_2 + \overline{f}_3 + \overline{f}_5 + \overline{f}_6\right),\\
\tau_{xy}^* &= -\rho^* u_x^*\left[u_y^* + \frac{1}{3}\right] + 2\left(\overline{f}_5 - \overline{f}_6\right).
\end{aligned} \tag{51}$$

6. Results for the two-dimensional lid-driven cavity flow problem

The incompressible flow in a square cavity whose top wall moves with a uniform velocity has been used as a model problem for testing and evaluating numerical techniques, in spite of the singularities we have at the two top corners. In this kind of flow problem, a main primary vortex is formed near the

center of the cavity and secondary or even tertiary vortices appear in the corners and are intensified when the Reynolds number (Re) increases (Figure 7).

In LBM framework, numerical solutions were based on the BGK model [16], multi-relaxation times [17], [18], entropic approach [19] and regularization [20], [21].

The purpose of this section is to show some numerical simulations that were performed to test the new proposed set of boundary conditions presented in Section 5 with respect to convergence, adherence, accuracy and stability.

Simulations were performed for Re= 100, 400, 1000, 3200 and 5000.

Accuracy was tested comparing our results with the classical results of Ghia et al. [22], who solved this problem using a multigrid method, based on the vorticity-stream $\omega - \psi$ formulation.

The Mach number (Ma) was taken as $Ma = u_0 / c_s$, where u_0 is the dimensionless lid velocity and $c_s = 1/\sqrt{3}$ is the speed of sound in the D2Q9 LBE. This result in the following relationship for the dimensionless relaxation time ω^{-1}

$$\omega^{-1} = \frac{LMa}{\mathrm{Re}\, c_s} + \frac{1}{2} \tag{52}$$

where L is the number of grid points along a coordinate x or y.

As pointed out in Sections 3-4, the numerical simulation with the D2Q9 LBE is restricted to incompressible flows, with errors $O\left(Ma^3\right)$. Therefore, we restrict the Mach number to $Ma = 0.1$ and Eq. (52) can be used to find the relaxation time ω^{-1} in terms of the Reynolds number and the number of grid points.

Convergence was tested by doubling, successively, the number of grid points: 32, 64, 128, 256 and 512. It was achieved with a small number of grid points of 128 for Re=100 and 400, but, as it was expected, higher Reynolds number required to increase this number.

Figure 8 and 9 show the numerical results for Re=400, 1000 and 5000 showing the relative velocity u_x/u_0 along the mid-line x=L/2 and the relative velocity u_y/u_0 along the mid-line y=L/2 of the cavity. Results were based on simulations performed using a 512^2 numerical domain. Adherence conditions for both y=0 and y=L are verified.

Results can be considered as accurate with respect to Ghia *et al.* [22] results.

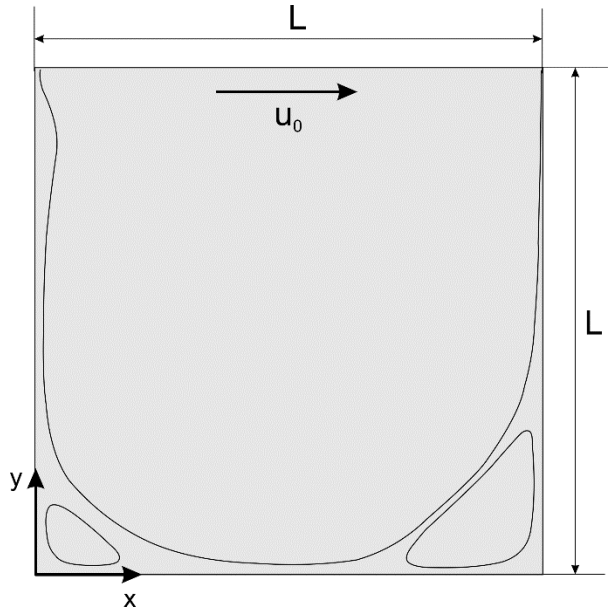

Figure 7. The two-dimensional cavity flow problem. The lid in y=L is moving with a constant velocity u_0 and produces a main vortex and two secondary vortex on the right and left bottom corners.

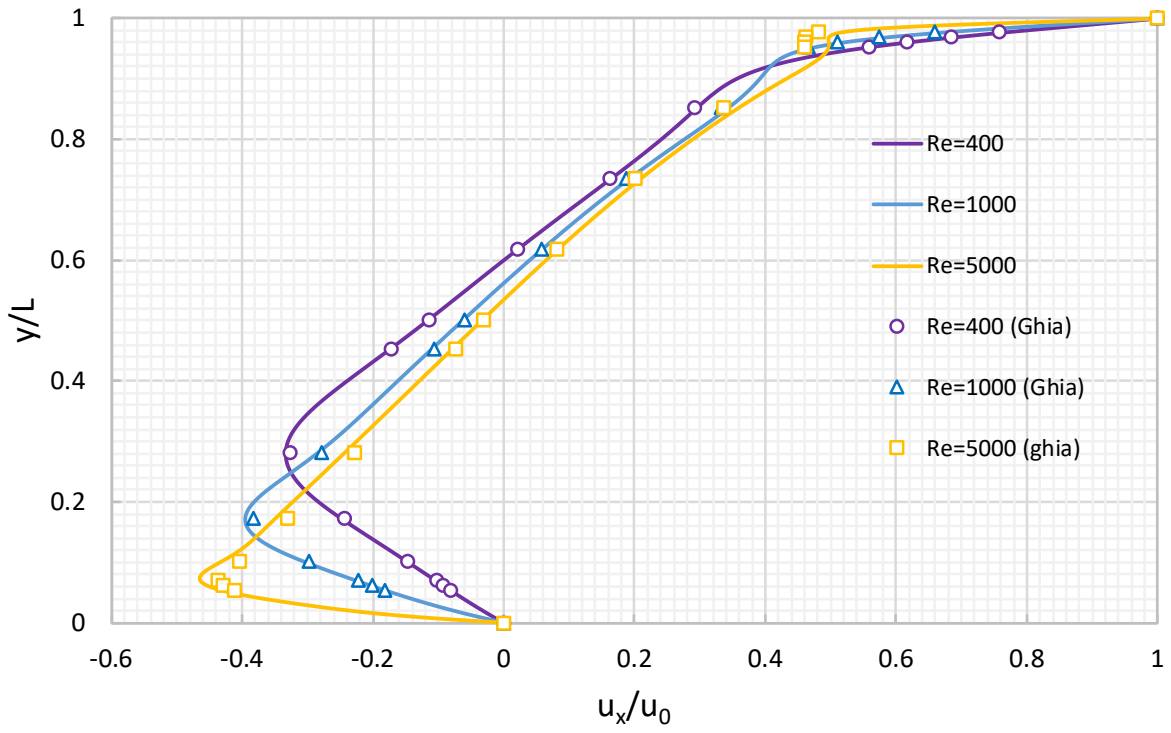

Figure 8. Numerical results for Re=400, 1000 and 5000 showing the relative velocity u_x/u_0 along the mid-line x=L/2. Simulations were performed using a 512^2 numerical domain. Adherence conditions for both y=0 and y=L are verified. Results are compared with Ghia *et al.* [22].

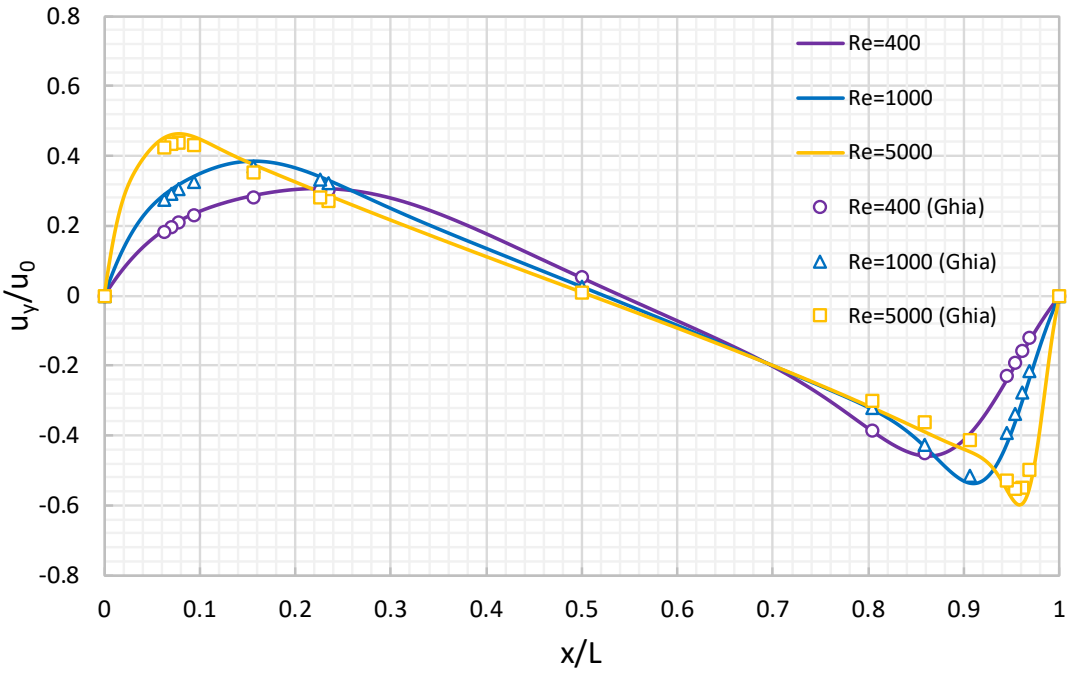

Figure 9. Numerical results for Re=400, 1000 and 5000 showing the relative velocity u_y/u_0 along the mid-line y=L/2 of the cavity. Simulations were performed using a 512^2 numerical domain. Adherence conditions for both x=0 and x=L are verified. Results are compared with Ghia *et al.* [22]

6.1. Stability

For the lid driven cavity, the Reynolds number can be written in terms of dimensionless parameters as

$$\mathrm{Re} = \frac{u_0^* L^*}{\nu^*} ,$$

where $u_0^* = u_o / c$ is the dimensionless lid velocity, c is the lattice speed, $c = h/\delta$, $L^* = L/h$ is the number *N* of lattice nodes along one of the two orthogonal direction and ν^* is the dimensionless kinematic viscosity

$$\nu^* = c_s^2 \left(\frac{1}{\omega} - \frac{1}{2} \right)$$

Therefore, for a given L^* the Reynolds number can be increased both by increasing the dimensionless lid velocity or by increasing the collision frequency till its upper limit 2. For each L^* and u_0^*, Figure 10 was built by reducing the relaxation time in such a way as to increase the Reynolds number till the stability limit of the lid driven cavity LB simulations. As it is to be expected high values of u_0^*, such as $u_0^* = 0.125$, reduces the stability limit. Nevertheless, for reasons that are still to be explained, very small values of u_0^*, such as $u_0^* = 0.015625$ has also the effect of lowering this stability limit. Values of u_0^* depicted in Figure 10 were found as $u_0^* = \frac{1}{c}$ where c=2^3, 2^4, 2^5, 2^6. In present simulations, the value of u_0^* leading to the larger stability limits was found in the intermediate range 0.03125-0.0625.

Figure 11 shows the results that were obtained for the stability of the proposed kinetic algorithm when compared with other works. We compare the stability range of the LB algorithm, when using the boundary conditions that were proposed in this paper, with the stability range of BGK based algorithms and with the work of Montessori *et al*. [20], who used the same regularized equations shown in Section 3, but wrote the boundary conditions in accordance with Guo *et al.* [9] model.

This comparison is performed for two lid dimensionless velocities $u_0^* = 0.125$ and $u_0^* = 0.03125$. It is clearly seen the beneficial effect the use of regularized boundary conditions has on the stability of the simulation algorithm, Indeed, even in the worst case, corresponding to $u_0^* = 0.125$, the stability range is multiplied by 2 in the lower resolution case ($L^* = 40$) and reaches four times the stability range of Montessori and co-workers in the larger resolution case ($L^* = 100$).

In addition, for the larger resolution ($L^* = 100$) a large improvement of the stability range was achieved, up to Re=85000, when the dimensionless lid velocity is reduced to $u_0^* = 0.03125$.

7. Conclusion

In LBM framework we deal with populations of particles and not with macroscopic quantities as in the Navier-Stokes level. Going back to Section 5, it is important to take into account that the pre-collisional populations outgoing from a boundary node into the fluid phase, were calculated following an algorithm that is based on the mass conservation of particles and on the regularization of the components of the viscous stress tensor.

By *regularization*, we mean that these components are calculated by replacing the unknown outgoing populations by their kinetic projections on the subspace generated by a second-order set of Hermite polynomials. This procedure results in a closed set of 4 equations for the unknows $\rho^*, \tau_{xx}^*, \tau_{yy}^*, \tau_{xy}^*$ and the solution of this set of equation enables to find the unknown pre-collisional populations in terms of the incoming populations (e.g., Eqs. (38) and (46)), without any heuristic assumptions and to regularize the incoming populations relieving these populations from errors due to high-order uncontrolled moments.

This idea can be easily extended to high order LBE and will be the subject of a next paper.

Acknowledgements.

PCP was partially funded by the Brazilian National Council for Scientific and Technological Development (CNPq).

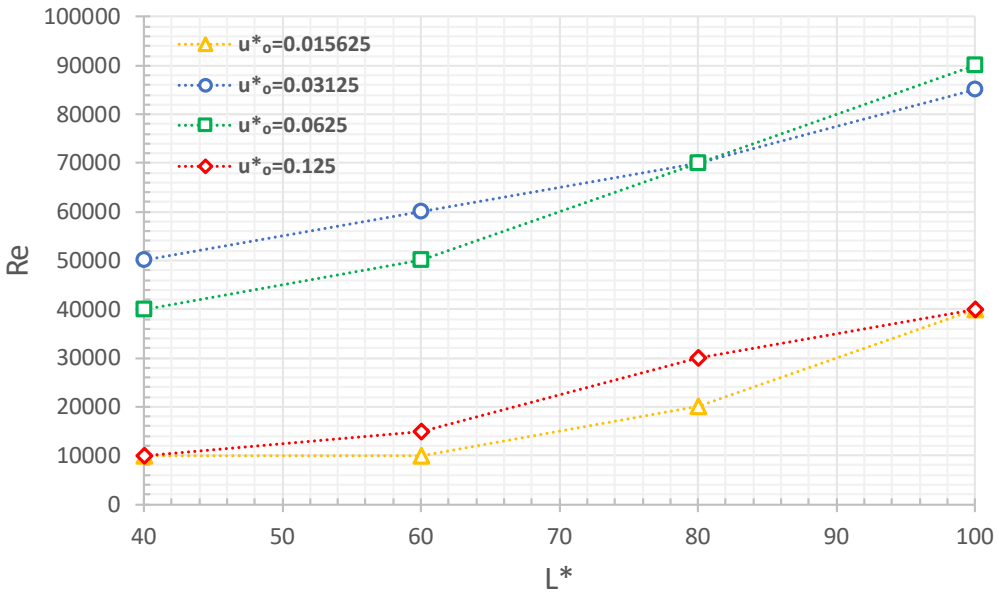

Figure 10. Stability limits for different values of the dimensionless velocity u_0^* and L^*.

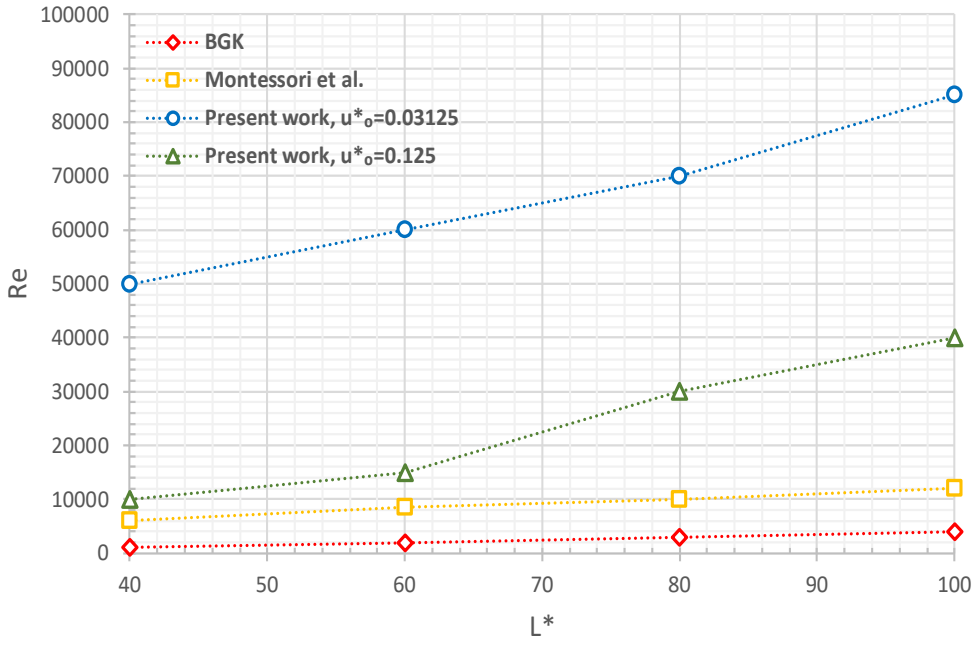

Figure 11. Stability ranges of the LB algorithm with regularized boundary conditions when compared to previous work. BGK and Montessori results were extracted from Montessori et al. [20].

References

1. Philippi PC, dos Santos LOE, Hegele LA, et al (2011) Thermodynamic consistency in deriving lattice Boltzmann models for describing segregation in non-ideal mixtures. Philos Trans R Soc A 369:2292–300. doi: 10.1098/rsta.2011.0021
2. Siebert DN, Philippi PC, Mattila KK (2014) Consistent lattice Boltzmann equations for phase transitions. Phys Rev E 90:053310. doi: 10.1103/PhysRevE.90.053310

3. Philippi PC, Mattila KK, Siebert DN, et al (2012) Lattice-Boltzmann equations for describing segregation in non-ideal mixtures. J Fluid Mech 713:564–587. doi: 10.1017/jfm.2012.473
4. Ladd AJC (1994) Numerical simulations of particulate suspensions via a discretized Boltzmann equation. Part 1. Theoretical foundation. J Fluid Mech 271:285. doi: 10.1017/S0022112094001771
5. Latt J, Chopard B (2006) Lattice Boltzmann method with regularized pre-collision distribution functions. Math Comput Simul 72:165–168. doi: 10.1016/j.matcom.2006.05.017
6. Mattila KK, Philippi PC, Hegele LA (2017) High-order regularization in lattice-Boltzmann equations. Phys Fluids 29:046103. doi: 10.1063/1.4981227
7. Zou Q, He X (1997) On pressure and velocity boundary conditions for the lattice Boltzmann BGK model. Phys Fluids 9:1591–1598. doi: 10.1063/1.869307
8. Inamuro T, Yoshino M, Ogino F (1995) A non-slip boundary condition for lattice Boltzmann simulations. Phys Fluids 7:2928. doi: 10.1063/1.868766
9. Guo ZL, Zheng CG, Shi BC (2002) Non-equilibrium extrapolation method for velocity and pressure boundary conditions in the lattice boltzmann method. Chinese Phys (Overseas Ed 11:366–374. doi: 10.1088/1009-1963/11/4/310
10. Latt J, Chopard B, Malaspinas O, et al (2008) Straight velocity boundaries in the lattice Boltzmann method. Phys Rev E 77:056703. doi: 10.1103/PhysRevE.77.056703
11. Philippi PC, Hegele Junior LA, Surmas R, et al (2007) From the Boltzmann to the lattice-Boltzmann equation: beyond BGK collision models. Int J Mod Phys C 18:556–565. doi: 10.1142/S0129183107010796
12. Philippi PC, Hegele Júnior LA, dos Santos LOE, Surmas R (2006) From the continuous to the lattice Boltzmann equation: The discretization problem and thermal models. Phys Rev E 73:056702. doi: 10.1103/PhysRevE.73.056702
13. Siebert DN, Hegele Júnior LA, Surmas R, et al (2007) Thermal lattice Boltzmann in two dimensions. Int J Mod Phys C 18:546–555. doi: 10.1142/S0129183107010784
14. Shan X, Yuan X-F, Chen H (2006) Kinetic theory representation of hydrodynamics: a way beyond the Navier-Stokes equation. J Fluid Mech 550:413–441. doi: 10.1017/S0022112005008153
15. Bhatnagar P, Gross E, Krook M (1954) A Model for Collision Processes in Gases. I. Small Amplitude Processes in Charged and Neutral One-Component Systems. Phys Rev 94:511–525. doi: 10.1103/PhysRev.94.511
16. Hou S, Zou Q, Chen S, et al (1995) Simulation of cavity flow by the lattice Boltzmann method. J Comput Phys 118:329–347.
17. Wu JS, Shao YL (2004) Simulation of lid-driven cavity flows by parallel lattice Boltzmann method using multi-relaxation-time scheme. Int J Numer Methods Fluids 46:921–937. doi: 10.1002/fld.787
18. Luo L-S, Liao W, Chen X, et al (2011) Numerics of the lattice Boltzmann method: Effects of collision models on the lattice Boltzmann simulations. Phys Rev E 83:056710. doi: 10.1103/PhysRevE.83.056710
19. Asinari P, Karlin I V. (2010) Quasiequilibrium lattice Boltzmann models with tunable bulk viscosity for enhancing stability. Phys Rev E 81:016702. doi: 10.1103/PhysRevE.81.016702
20. Montessori a., Falcucci G, Prestininzi P, et al (2014) Regularized lattice Bhatnagar-Gross-Krook model for two- and three-dimensional cavity flow simulations. Phys Rev E 89:053317. doi: 10.1103/PhysRevE.89.053317
21. Hegele LA, Scagliarini A, Sbragaglia M, et al (2018) High-Reynolds-number turbulent cavity flow using the lattice Boltzmann method. Phys Rev E 98:043302. doi: 10.1103/PhysRevE.98.043302
22. Ghia U, Ghia KN, Shin C. (1982) High-Re solutions for incompressible flow using the Navier-Stokes equations and a multigrid method. J Comput Phys 48:387–411. doi: 10.1016/0021-9991(82)90058-4